AFOSR-TR-97
0033

Final Report on

Multiple Scale Methods for Stability Analysis of Fluid-Structure Systems

From September 15, 1992 - September 14, 1993

by

Professor Wing Kam Liu

Principal Investigator

Northwestern University

Department of Mechanical Engineering

2145 Sheridan Road

Evanston, Illinois, 60208

AFOSR Grant Number F49620-92-J-0505

DISTRIBUTION STATEMENT A
Approved for public release;
Distribution Unlimited

19970117 060

DTIC QUALITY INSPECTED 1

REPORT DOCUMENTATION PAGE

Form Approved
OMB No. 0704-0188

Public reporting burden for this collection of information is estimated to average 1 hour per response, including the time for reviewing instructions, searching existing data sources, gathering and maintaining the data needed, and completing and reviewing the collection of information. Send comments regarding this burden estimate or any other aspect of this collection of information, including suggestions for reducing this burden, to Washington Headquarters Services, Directorate for Information Operations and Reports, 1215 Jefferson Davis Highway, Suite 1204, Arlington, VA 22202-4302, and to the Office of Management and Budget, Paperwork Reduction Project (0704-0188), Washington, DC 20503.

1. AGENCY USE ONLY (Leave blank)	2. REPORT DATE	3. REPORT TYPE AND DATES COVERED
	1/94	Final 9/15/92 - 9/14/93

4. TITLE AND SUBTITLE
Multiple Scale Methods for Stability Analysis of Fluid-structure Systems

5. FUNDING NUMBERS

6. AUTHOR(S)
Wing K Liu

7. PERFORMING ORGANIZATION NAME(S) AND ADDRESS(ES)
Department of Mechanical Engineering
Northwestern University
2145 Sheridan Road
Evanston, IL 60208

8. PERFORMING ORGANIZATION REPORT NUMBER

9. SPONSORING MONITORING AGENCY NAME(S) AND ADDRESS(ES)
AFOSR
110 Duncan Avenue, Suite B#115
Bolling AFB, DC 20332-0001

10. SPONSORING MONITORING AGENCY REPORT NUMBER
F49620-92-J-0505

11. SUPPLEMENTARY NOTES

12a. DISTRIBUTION AVAILABILITY STATEMENT

12b. DISTRIBUTION CODE
Approved for public release;
Distribution unlimited

13. ABSTRACT *(Maximum 200 words)*

Multiple scale methods, which are based on discrete and continuous reproducing kernels, wavelets, and integral window transforms are developed . In this development, a microscope is constructed with a flexible space-time localized window function which translates and dilates in space and time to cover the entire domain of interest. This microscope can magnify, examine, and record the image of the various scales and frequencies of the response locally within the support of the window function. The degree of magnification will depend on the power of the microscope, a flexible space-scale and time-frequency window function. This complete characterization of the unknown response is performed through the integral window transform. This localization process can be achieved by dilating the flexible multiple-scale window function. The zoom in and zoom out capability of the window function is especially useful in examining complex flow phenomena, such as flow induced vibration, dynamic stability of flow-structure interaction, turbulence structures, and high frequency structural dynamics response.

14. SUBJECT TERMS
Dynamic Response, flow-structure interaction, kernel particle methods, multi-scale window function, wavelet

15. NUMBER OF PAGES
29 31

16. PRICE CODE

17. SECURITY CLASSIFICATION OF REPORT	18. SECURITY CLASSIFICATION OF THIS PAGE	19. SECURITY CLASSIFICATION OF ABSTRACT	20. LIMITATION OF ABSTRACT
unclssified	unclassified	unclaasified	unlimited

Reproducing Kernel and Wavelet Particle Methods

Wing Kam Liu, Fellow

and

Claus Oberste-Brandenburg

Northwestern University

Department of Mechanical Engineering

2145 Sheridan Road

Evanston, Illinois, 60208

Presented at the 1993 ASME Winter Annual Meeting, New Orleans. Appeared in the Book "Aerospace Structures: Nonlinear Dynamics and System Response" Eds. J. P. Cusumano, C. Pierre, and S. T. Wu. ASME, AD-Vol. 33, p. 39-56, 1993.

This research is supported by AFSOR Grant number F49620-92-J-0505

Abstract

Multiple scale methods, which are based on discrete and continuous reproducing kernels, wavelets, and integral window transforms are developed . In this development, a microscope is constructed with a flexible space-time localized window function which translates and dilates in space and time to cover the entire domain of interest. This microscope can magnify, examine, and record the image of the various scales and frequencies of the response locally within the support of the window function. The degree of magnification will depend on the power of the microscope, a flexible space-scale and time-frequency window function. This complete characterization of the unknown response is performed through the integral window transform. This localization process can be achieved by dilating the flexible multiple-scale window function. The zoom in and zoom out capability of the window function is especially useful in examining complex flow phenomena, such as flow induced vibration, dynamic stability of flow-structure interaction, turbulence structures, and high frequency structural dynamics response.

1. Introduction

In a compressible flow-structure system, the unstable response often arises from a coupling between phenomena associated with substantially different frequencies. For example, vortex formation in a flow about a blade or an airfoil is initiated by relatively high frequency modes of the structure. The excitation forces generated by the vortex and the instability itself generally involve low modes of structural response. The complete time integration of the equations for the compressible fluid and structure combined can be prohibitively time-consuming in even two dimensions and is beyond the capability of even the largest supercomputers in three dimensions. Thus it can be seen that methods which can effectively treat problems with large ranges in scale are needed in many types of analysis which arise in structural dynamics problems.

The development of computational methods for low-frequency response 3D structural systems are now reasonably well established. On the other hand, little success has been made in the structural area characterized by multiple scales, where response is often dominated by the middle part of the spectrum. The author believes that the multiple-scale reproducing kernel particle methods coupled with wavelets proposed here have great promise in dealing effectively with the difficult structural response problems in which the medium frequencies are important, such as problems involving impact, dynamic instability, compressible flow-structure interaction, and other local phenomena.

Because the frequency shift enables the time step to depend only on the size of the frequency band and *not* on the frequency extent of the load, these methods will speed up analysis of medium frequency response immensely. This is particularly attractive for structural response exhibiting multiple time scales. This new development will enable engineers not only to bring more detail into their structural system models, but will also enhance the computer simulations of many classes of multi-scale structural dynamics analysis. It will improve the accuracy, efficiency, and reliability of dynamic analysis.

In the next section, a review of the coupled compressible flow-structure interaction is presented. In section 3, the weak form of the equations of motion is given and some currently available solution methods are discussed. In section 4a, the discrete orthogonal reproducing kernel interpolation functions are reviewed. In section 4b, the multi-resolution wavelets analysis is given. In section 5, we present our proposed approach to study complex structures, the multiple scale reproducing kernel particle methods. Sample examples are given in section 6.

2. Review of Coupled Compressible Flow-Structure Interaction

The ability to solve general classes of fluid-structure interaction problems involving finite deformations and stability depends upon the ability to solve the corresponding uncoupled fluid and structural problems, and also the ability to interface fluid and structural subdomains. During the last two decades, considerable progress has been made in the solutions of free and moving boundary problems which involve large fluid deformations. Among these methods are the marker-and-cell (MAC) methods (Hirt [1975, 1983], Nichols and Hirt [1971], Harlow and Welch [1965]), the volume of fluid (VOF) methods (Amsden and Harlow [1970], Harlow et al. [1976]), moving mesh techniques (Subbiah et al [1989]), Eulerian and arbitrary Lagrangian-Eulerian (ALE) methods (Liu et al. [1988, 1991], Huerta and Liu [1988], Belytschko [1983], Belytschko and Kennedy [1978]), the smoothed particle hydrodynamic (SPH) methods and the free Lagrange methods (Monaghan and Gingold [1983], Gingold and Monaghan [1982], Burton and Harrison [1991]). However, the coupling of these methods with deformable structures is not well understood and often causes difficulties.

In the MAC method, a fixed or Eulerian mesh is used for the fluid calculation and a Lagrangian set of marker particles is used to trace the moving free surface. Marker particles can be spread over all fluid occupied regions with each particle specified to move with the fluid velocity at its location. A free surface is defined as lying at the "boundary" between regions with and without marker particles. More specifically, a mesh is said to contain a free surface if the mesh contains cells with markers and has at least a neighboring cell with no markers. The MAC method offers the distinct advantage of eliminating all logic problems associated with intersecting surfaces. This method is also readily extendable to three dimensional computations. However, the MAC method requires significant increase in running time and storage.

In the VOF approach, a function F is defined whose value is unity at any point fully occupied by fluid and zero otherwise. Cells with F values between zero and one must then contain a free surface. This fractional volume of fluid (VOF) method provides the same coarse interface information available in the marker particle method. In order to trace the free surface, a flow analysis network approach is developed. It uses the flux calculation at the boundary of each control volume to check the fraction of fill instead of tracking marker particles. One limitation of this control volume technique is that the time step must be controlled to ensure that free surface only passes one control volume in a time step.

In a moving mesh approach, a numerical grid generation scheme, which facilitates solutions over arbitrarily shaped boundaries, has to be developed. This approach numerically maps the irregular shape of the flow field to a more regular shape in a computational domain

where the governing equations are solved. The computation time of this method is relatively high because of the large number of time steps and the mesh generation at each time step.

There are two approaches to ALE methods. One approach updates the solution variables in a single time step while the other performs a Lagrangian step follows by an Eulerian or remap (or advection) step. The latter strategy is often referred to as an operator split method. Similar to the moving mesh approach, a new mesh is required for the ALE calculations. However, this new mesh is required only if the Lagrangian mesh is too distorted. The major advantage of the ALE methods is the moving boundaries can be computed with high accuracy of the Lagrangian method, and the mesh can conserve its regularity in avoiding element entanglement. Although a combination of multi-material ALE methods have also been developed, the application of this technique to multiple free surfaces, multiple materials, and fluid-structure interaction remains to be explored.

The SPH (smooth particle hydrodynamics) and the free Lagrange methods are based on algorithms which are truly grid-free or mesh-free. Consequently, these techniques do not have the mesh entanglement problems and at the same time, maintain the high accuracy of the Lagrangian calculations. Similar to a finite difference/element Lagrangian calculation, the continuous fluid is approximated by a set of particles or fluid elements of equal mass. Unlike the traditional Lagrangian finite element/difference calculations, the inter-particle forces among these smooth fluid particles are derived from the pressure and these interacting pressure forces are governed by an interpolating function. Hence, the nodal or element forces (which are usually constructed from a finite element/difference mesh) are no longer needed; and consequently, these free Lagrange methods require no mesh and the mesh distortion problems are completely eliminated. The energy equation is similarly defined for each smooth fluid particle. Since the fluid is modeled by equal mass particles, the density for the fluid is constructed by defining a weighting function in which the density of the equal mass particles is proportional to the number of particles per unit volume. With these approximations, the motion of the fluid is governed by the movement of this set of smooth fluid particles, and the movement of the particles are governed by the particle interacting forces.

Although SPH methods work well if there is no boundary (since the boundary terms are tossed out in the formulation, Libersky and Petschek [1990]), and when the number of unknowns (nodes) is large; SPH methods are not as accurate as the regular finite element methods, Johnson, Peterson and Stryrk, [1993]. From our study of SPH interpolation function via a simple one dimensional (1D) Galerkin formulation, we found that there is an additional deficiency in the SPH formulation. It is related to the boundary correction term of the reproducing kernel approximation. We shall make an attempt to identify this deficiency and present our view of improving the SPH kernel approximation.

After reviewing the moving least square interpolation functions, Lancaster and Salkauskas [1981], and the diffuse element methods (DEM), Nayroles et al. [1992]. Belytschko et al. [1993] pointed out that an assumption made by Nayroles et al., the interpolation coefficients are constants, detracts from the accuracy of the method. They developed the Element Free Galerkin Methods (EFGM) and showed that by adding more accurate derivatives and enforcing boundary conditions by Lagrange multipliers, the methods could achieve very high rates of convergence. From our experience, EFGM are more accurate than the finite element methods, and hence, the SPH methods especially for a small set of nodes. One main drawback of EFGM is the computational expense, and we found that it is more computationally intensive than the SPH methods.

The objective of the Reproducing Kernel Particle Methods developed by Liu et al. [1993], is along the same line of development as the SPH, DEM, and EFGM : to develop an accurate and efficient mesh free interpolation functions. A detailed discussion on smooth particle methods, the diffuse element methods and the element free Galerkin method, and the recently developed reproducing kernel particle methods, is also given in the paper.

Since a continuous reproducing kernel can be derived for this method and it is also a free Lagrange particle method, we shall label this development as *Reproducing Kernel Particle Methods* (RKPM). This proposed approach is motivated by the theory of wavelets Chui [1992] and Daubechies [1992], in which a function is represented by a combination of the dilation and translation of a single wavelet, which is a window function. In a wavelet analysis, similar to the SPH interpolation kernel, the interpolation coefficients are defined in terms of the integral window transform of the window function and the solution itself. In this proposed study, we shall make use of the multiple frequency bands and/or multiple scales properties of wavelets analysis (multi-resolution analysis), and the time-frequency and/or space-scale localization properties of the continuous and discrete reproducing kernel approximations.

3. Weak Form of the Equation of Motion and Solution Methods

Consider the weak form of the equations of motion which can be written as:

$$K\langle \delta u^h, u^h\rangle + B\langle \delta u^h(x\varepsilon\Gamma_g), u^h(x\varepsilon\Gamma_g) - g(x)\rangle = f\langle \delta u^h, p\rangle \qquad (3.1)$$

where $K\langle\cdot, \cdot\rangle$, $B\langle\cdot, \cdot\rangle$ and $f\langle\cdot, \cdot\rangle$ are the usual weak form operator of the governing equations, boundary constraint operator on Γ_g, and the force assembly operator, respectively. $\delta u^h(x, t)$, $u^h(x, t)$, $p(x, t)$ and $g(x, t)$ are the test function, trial function, body force, and prescribed data on the boundary Γ_g. The governing equations can be those of structural

dynamics, fluid dynamics, coupled-fluid-structure interaction or structural acoustics, and among others. The classical Galerkin method is to approximate u^h (which is the approximation to u(x, t)) by:

$$u^h(x, t) = \sum_{a=1}^{A} C_a \phi(x - x_a) \tag{3.2a}$$

and

$$\delta u^h(x, t) = \sum_{a=1}^{A} \delta C_a \phi(x - x_a) \tag{3.2b}$$

where $\phi(x - x_a)$ can be the global finite element shape functions, Hughes [1987], spectral functions Gottlieb and Orszag [1977], the smooth particle hydrodynamic (SPH) interpolation kernel function, Lucy [1977] and Monaghan [1988], multiple scale finite element functions Liu, Zhang and Ramirez [1991], or wavelet-type bases, Chui [1992] and Daubechies [1992], etc. Substitute Eqs. (3.2) into Eq. (3.1) and solve for C_a for a = 1, ..., A coefficients will result in the discrete approximation of u(x), provided certain continuity requirements are met.

It is noted that the above solution procedures also hold for the various approaches such as the space-time discontinuous finite elements, Hughes and Hulbert [1988], and Shakib and Hughes [1991], deforming space-time discontinuous finite elements, Tezduyar, Behr and Liou [1992]; the arbitrary Lagrangian-Eulerian (ALE) and Eulerian-type finite element methods, Liu et al. [1991], and among others. All these methods employ the same type of interpolations, Eqs. (3.2), except a new set of motion, mesh motion, is introduced through similar equations (3.2). This additional motion is used to control the mesh or grid deformation so that mesh distortion can be minimized and the nodal points connectivity through the mesh or grid description would not give negative Jacobians, Liu et al. [1988].

Equations (3.2) give a good approximation to u(x, t) when the measure of the spacing among x_a, call it h, becomes smaller and smaller. One can then visualize the coefficient C_a as an average value of u(x, t), and $\phi(x - x_a)$ is the weighting function. If h approaches to zero C_a approaches to the true solution at x_a. However, in practice, h does not approach zero and if u(x, t) is a very nonlinear function, solving for the average values, as all of these methods do, would probably leave out the fine details of the response u(x, t).

Therefore, our objective is, instead of solving for the averaged $u(x_a)$ (i.e., C_a), we shall develop an alternative form of Eqs. (3.2), which is based on discrete reproducing kernels and

integral window transforms. In this approach, if we include the time dimension into $\mathbf{x}$, we can think of $\phi(\mathbf{x} - \mathbf{x}_a)$ as a flexible space-time window function located at $\mathbf{x}_a$. Since $u(\mathbf{x})$ is an unknown function, our goal then is to interpret the coefficient C_a as a microscope which magnifies, examines, and records the image of the response $u(\mathbf{x})$ around $\mathbf{x}_a$. This can be achieved by employing a space-time localized window function that can recover the various scales and frequencies of the response $u(\mathbf{x})$ locally around $\mathbf{x}_a$. This leads us to the use of scaling functions and wavelets which are discussed in the next two sections.

4a. Discrete Orthogonal Reproducing Kernel Interpolation Functions

If $\phi(\mathbf{x} - \mathbf{x}_a)$ is chosen to be the scaling function, Chui [1992], C_a is identified as the integral window transform of the unknown response u and $\phi(\mathbf{x} - \mathbf{x}_a)$ over the domain. That is, the unknown coefficients are to be constructed so that:

$$C_a = C_a(u, \mathbf{x}_a) = \langle u, \phi_a \rangle = \int_V u(\mathbf{x})\, \phi(\mathbf{x}-\mathbf{x}_a)\, d\mathbf{x} \tag{4.1}$$

where $\langle u, \phi_a \rangle$ is the integral window transform, and V is the domain of interest. The reconstruction formula Eq. (3.2a) becomes:

$$u^h(\mathbf{x}, t) = \sum_{a=1}^{A} \langle u, \phi_a \rangle\, \phi(\mathbf{x}-\mathbf{x}_a) \tag{4.2}$$

Equation (4.2) is typical for a discrete reproducing kernel Hilbert space. In seeking for the solution $u^h(\mathbf{x}, t)$ using Eq. (4.2) and a similar equation for $\delta u^h(\mathbf{x})$, it is necessary to define nodal point $\mathbf{x}_J$; nodal $u_J \equiv u(\mathbf{x}_J)$; and particles with nodal mass ΔM_J and nodal density ρ_J. Consequently, the nodal volume ΔV_J is determined by $\Delta M_J/\rho_J = \Delta V_J$ for J = 1, ..., NP, where NP is the total number of particles inside V. Hence,

$$\sum_{J=1}^{NP} \Delta V_J = V \;; \quad \text{and} \quad \sum_{J=1}^{NP} \Delta M_J = \text{total mass} \tag{4.3}$$

Using numerical integration in Eqs. (4.2) and the above definitions, $u^h(\mathbf{x}, t)$ becomes:

$$u^h(\mathbf{x}, t) = \sum_{a=1}^{A} \langle u, \phi_a \rangle\, \phi(\mathbf{x}-\mathbf{x}_a)$$

$$= \sum_{a=1}^{A} \left[\sum_{J}^{x_J \in B(x_a)} \phi(x_J - x_a) \Delta V_J \, u_J(t) \right] \phi(x - x_a) \tag{4.4}$$

where x_J are the quadrature points, and $B(x_a)$ is the support of $\phi(x-x_a)$. Equation (4.4) is a discrete reproducing kernel approximation (DRKA), since $u^h(x, t)$ is interpolated via $\phi(x-x_a)$ through the integral window transform of $u(x, t)$. An interesting interpretation of Eq. (4.4) is as follows. There are a total of A sampling windows spread over the domain V. At each sampling location x_a, a microscope, which is constructed from the integral window transform $<u, \phi_a>$, examines the motion of particles ΔM_J carrying nodal values u_J passing through the support $B(x_a)$. If the motion is very nonlinear, the number of "*free Lagrange particles*" ΔM_J passing through each sampling window $\phi(x-x_a)$ is different from time to time. Therefore, Eq. (4.4) maintains the attributes of the free Lagrange methods, and with the appropriate choice of $\phi(x-x_a)$, gives more accurate results.

Upon examining Eq. (4.4), since only a set of nodal points or particles are involved in DRKA methods, similar to SPH methods, DRKA methods have no problems associated with mesh/grid distortion or negative Jacobian of the elements resulting from large deformation. Hence, it is suitable for large deformation and high velocity flow problems. However, unlike SPH methods in which $\phi(x-x_a)$ in Eq. (3.2a) is the interpolation kernel function that mimic a Dirac Delta function and C_a is the product of the nodal mass ΔM_a and the nodal value of the response u_a ($\approx u(x_a)$) divided by the nodal density ρ_a, (Monaghan [1988]). That is

$$u^h(x, t) = \sum_{a=1}^{A} \phi(x-x_a) \frac{\Delta M_a}{\rho_a} u_a \equiv \sum_{a=1}^{A} \phi(x-x_a) \, \Delta V_a u_a \tag{4.5}$$

Comparing Eqs. (4.4) and (4.5), if only one point integration is used to integrate the integral window transform $<u, \phi_a>$, which is a very bad approximation to the integral, especially for very nonlinear or complex $u(x, t)$, the SPH and DRKA methods take a similar form. However, if more than one point quadratures are employed to evaluate the integral window transform $<u, \phi_a>$, the difference between the two methods is apparent. It is thus clear from Eq. (4.4) why we call C_a a microscope in which the magnification power will depend on the number of particles examined under the support $B(x_a)$.

4b. Multi-Resolution Wavelets Analysis

In this section, we wish to construct and interpret C_a as a *flexible* power microscope. This microscope can zoom in (sharpen the window function) to pick up the detailed structures of the response $u(x)$; and zoom out (widen the window function) if no further magnification of the response is necessary. This zoom in and zoom out capability is especially useful in examining complex flow phenomena, such as flow induced vibrations; dynamic stability of flow-structure interaction, turbulence structures, structural acoustics, high frequency structure dynamic response, strain localization problems, and other engineering disciplines.

In this development, since C_a is defined in terms of the unknown response $u(x)$ and the multiple scale window function $\phi(x-x_a)$, Eq. (4.2) has to be redefined for the multi-resolution wavelets analysis. The window functions $\phi(x-x_a)$ will be replaced by flexible power window functions $\psi_{ma}(x)$; whereas the integral window transform coefficients $C_a = \langle u, \phi_a \rangle$, a = 1, ..., A, become C_{ma}, which are defined by $\langle u, \psi_{ma} \rangle$. The power of the window function is controlled by an index m = 0, 1, ..., M. The multi-resolution analysis is performed simply by the dilation of the window functions. That is, the discrete reproducing kernel formula Eq. (4.2) can be re-defined as:

$$u^h(x) = \sum_{m=0}^{M} \sum_{a=1}^{Am} \langle u, \psi_{ma} \rangle \psi_{ma}(x) = \sum_{m=0}^{M} \sum_{a=1}^{Am} C_{ma} \psi_{ma}(x) \tag{4.6a}$$

where the dilation of $\psi_{ma}(x)$ is defined through the integer index m, and A0 > A1 > .... > AM. The arbitrary scale, $a_0 > 0$, is usually set equal to 2. Hence, the flexible space-time and scale-frequency window functions are defined by:

$$\psi_{ma}(x) = a_0^{-m/2} \psi(a_0^{-m}(x-x_a)) \qquad a_0 > 0 \tag{4.6b}$$

and the integral window transform $\langle u, \psi_{ma} \rangle$ is given by:

$$C_{ma} = \langle u, \psi_{ma} \rangle = \int_V \psi_{ma}(x)\, u(x)\, dx \tag{4.6c}$$

where V is the space (or space-time) domain of interest.

As can be seen from Eq. (4.6b), the mother wavelet $\psi(x)$ can be obtained by setting m = 0 and $x_a = 0$. Because of our choice of indexing, m = 0 corresponds to the smallest window width. The integral window transform $\langle u, \psi_{0a} \rangle$, the microscope, can pick up the very fine scale and/or high frequencies up to the arbitrary scale a_0. For m = M, it corresponds to the

largest window width, and $C_{Ma} = \langle u, \psi_{Ma} \rangle$, the microscope, can pick up the large scale and/or low frequency response.

It is apparent from Eqs. (4.6) that the microscope C_{ma} located at x_a can examine the finest scales of $u(x)$ simply by dilation. The magnification factor is determined by the mother window function, and the flexible space-scale and time-frequency localized integral window transform $\langle u, \psi_{ma} \rangle$.

Using a numerical quadrature integration scheme to discretize Eq. (4.6c) gives:

$$C_{ma} = \langle u, \phi_{ma} \rangle = \sum_{J}^{x_J \epsilon B^m(x_a)} \psi_{ma}(x_J)\, \Delta V_J\, u_J \tag{4.7a}$$

where $B^m(x_a)$ is the support of the m^{th} scale window function located at x_a and ΔV_J is the J^{th} nodal volume evaluated at x_J. Substituting Eq. (4.7a) into Eq. (4.6a), we obtain our desired discrete multi-resolution wavelet analysis of $u(x)$:

$$u^h(x) = \sum_{m=0}^{M} \sum_{a=1}^{Am} \left\{ \sum_{J}^{x_J \epsilon B^m(x_a)} \psi_{ma}(x_J)\, \Delta V_J\, \psi_{ma}(x) \right\} u_J \tag{4.8}$$

Similar equation can also be written for $\delta u^h(x)$. Equation (4.8) can be written in a more familiar form of multi-resolution analysis:

$$u^h(x) = \sum_{m=0}^{M} u^h_m(x) = u^h_0(x) + u^h_1(x) + \cdots + u^h_M(x) \tag{4.9a}$$

It can be seen from Eq. (4.7a) that $u^h(x)$ is a direct sum of the M-scale solution. For each refinement m, the m^{th}-scale interpolation, which also represents the m^{th}-frequency/wave number band of the solution, is defined by:

$$u^h_m(x) = \sum_{a=1}^{Am} u^h_{ma}(x) = u^h_{m1}(x) + u^h_{m2}(x) + \cdots + u^h_{mAm}(x) \tag{4.9b}$$

From Eq. (4.9b), we can view each $u^h_{ma}(x)$ as a flexible power microscope examining $u(x)$ around x_a and each $u^h_{ma}(x)$ is interpolated through the window function so that:

$$u^h_{ma}(x) = \sum_{J}^{x_J \varepsilon B^m(x_a)} N_{maJ}(x)\, u_J \tag{4.9c}$$

and the m^{th} scale-a^{th} wavelet shape function ($N_{maJ}(x)$) of particle J is given by (no sum on m, a and J):

$$N_{maJ}(x) = \psi_{ma}(x_J)\, \Delta V_J\, \psi_{ma}(x) \tag{4.9d}$$

From Eq. (4.9c), the summation on J for $x_J \varepsilon B^m(x_a)$ will define the global nodal connectivity. However, unlike the usual finite element, the sequence of numbering u_J would not cause any mesh distortion or negative Jacobian problems since there is no element.

If additional particles are added to the domain (this can easily be done by splitting up particles), the adaptive multi-resolution analysis can be summarized as follows:

$$u^h(x) = \sum_{m=0}^{M} u^h_m(x) \qquad \text{multi-resolution analysis} \tag{4.10a}$$

$$= \sum_{m=0}^{M} \left(\sum_{a=1}^{Am} u^h_{ma}(x) \right) \qquad \text{summation of all frequency bands of interest} \tag{4.10b}$$

$$= \sum_{m=0}^{M} \left(\sum_{a=1}^{Am} \left[\sum_{J}^{x_J \varepsilon B^m(x_a)} N_{maJ}(x)\, u_J \right] \right) \qquad \begin{array}{l} u_J \text{ are examined by the } m^{th} \text{ scale-} a^{th} \\ \text{wavelet under } B^m(x_a) \end{array} \tag{4.10c}$$

$$= \sum_{J}^{x_J \varepsilon B^m(x_a)} \left\{ \sum_{m=0}^{M} \sum_{a=1}^{Am} \left(\psi_{ma}(x_J) \Delta V_J \psi_{ma}(x) \right) \right\} u_J \qquad \text{global interpolation functions} \tag{4.10d}$$

As can be seen, there is no change in the multi-resolution analysis Eqs. (4.10a) and (4.10b), since the dilation index m and the number of window functions $\psi_{ma}(x)$ are the same. There is also no change in the order of the window function as $\psi_{ma}(x)$ is derived from $\psi_{0a}(x)$. The only change is in the summation on J under the support $B^m(x_a)$ and the resulting "*nodal/particle*" matrix will be larger because of the additional global interpolation functions of those nodes/particles. Similar procedures can also be developed for the deletion of particles.

If we can construct discrete multi-resolution wavelet functions according to Eqs. (4.10), we shall have a *truly mesh or grid-free adaptive* method and the interpolation is defined through a set of arbitrary-spaced nodal points or particles. Moreover, if $\psi(x)$ is chosen to be C^k smooth functions, i.e., smooth in its k^{th} derivatives, the discrete multi-resolution reproducing kernel interpolation functions are also C^k.

5. Multiple Scale Reproducing Kernel Particle Methods

The multi-resolution wavelet analysis given in sections 4 is based on an infinite domain assumption. To apply wavelets to analyzing complex structures, this restrictive assumption is no longer valid. Another intrinsic deficiency of orthogonal wavelet is the stringent requirement:

$$\int x^m \psi(x) dx = 0 \qquad m = 0, 1, ..., q \tag{5.1}$$

where q is the degree of polynomials of the mother wavelet $\psi(x)$. From Eq. (5.1) it follows that a q^{th} order wavelet can not represent 1, x, x^2, ..., x^q, parts of the solution. To remedy these two restrictions, we shall represent a function u(x) by:

$$u(x) = u^w(x) + \mathbf{P}(x)\mathbf{c} \tag{5.2}$$

where $u^w(x)$ is the part of the solution that is obtained by the multi-resolution wavelet reconstruction as given in section 4b. $\mathbf{P}(x)= \{P_1(x), P_2(x), ..., P_n(x)\}$ and $\mathbf{c} = \{c_1, c_2, ..., c_n\}^T$ are the vectors of the n linear independent functions and unknown coefficients, respectively. A superscript T denotes the transpose. We can consider the $\mathbf{P}(x)\mathbf{c}$ term as the residual representation of u(x) within a bounded domain. Following the procedures of deriving the reproducing kernel particle interpolation functions (see Liu et al.[1993]), the multiple scale reproducing kernel interpolation function coupled with wavelets can be shown to be:

$$u(x) = u^w(x) + \int_v C(x, y, a_0)\, a_0^{-1}\, \phi\left(\frac{y-x}{a_0}\right) u(y)\, dy$$

$$- \int_v C(x, y, a_0)\, a_0^{-1}\, \phi\left(\frac{y-x}{a_0}\right) u^w(y)\, dy \tag{5.3}$$

where the parameter a_0 determines the size of the scaling function $\phi(x)$. The form of the correction function $C(x, y, a_0)$ will depend on the choice of $P(x)$. It is noted that the second term in Eq.(5.3) is the reproducing kernel approximation described in Appendix A. The first term is the multi-resolution wavelet part, whereas, the third term *connects* the two reproducing methods. It is interesting to point out that by a proper choice of a_0, the contribution of the coupling term can be shown to be negligible. With this construction, the wavelet and the reproducing kernel terms give the high and low frequency (or the fine and coarse scales) representations of the solution u. It is also noted that $u^w(x)$ can be expressed by other continuous or discrete multiple scale reproducing kernels.

To further examine this multiple frequency/wave number bands wavelet approximation, we let

$$u^w(x) = \sum_{m=0}^{M} \sum_{a=1}^{Am} \langle u, \psi_{ma} \rangle \psi_{ma}(x) \tag{5.4}$$

Substituting Eq.(5.4) into Eq. (5.3) yields:

$$u(x) = \sum_{m=0}^{M} \sum_{a=1}^{Am} \left\{ \int_v u(y)\, \psi_{ma}(y)\, dy \right\} [\psi_{ma}(x) - \tilde{\psi}_{ma}(x)]$$

$$+ \int_v C(x, y, a_0)\, a_0^{-1}\, \phi\left(\frac{y-x}{a_0}\right) u(y)\, dy \tag{5.5}$$

where the definition of:

$$\langle u, \psi_{ma} \rangle = \int_v u(y)\, \psi_{ma}(y)\, dy \tag{5.6a}$$

has been used in Eq.(5.5). The approximation of the wavelet functions $\psi_{ma}(x)$ through the reproducing kernel, denoted by $\tilde{\psi}_{ma}(x)$ is:

$$\tilde{\psi}_{ma}(x) = \int_v C(x, y, a_0)\, a_0^{-1}\, \phi\left(\frac{y-x}{a_0}\right) \psi_{ma}(y)\, dy \tag{5.6b}$$

It is now clear from Eq. (5.6b) that $\tilde{\psi}_{ma}(x)$ is simply an approximation of $\psi_{ma}(x)$ via the reproducing kernel reconstruction. It is expected that $\tilde{\psi}_{ma}(x)$ is very close to $\psi_{ma}(x)$ for low frequency/wave number wavelets. Consequently, the contribution from the low frequency/wave number wavelets is close to zero. However, depending on the choice of a_0, ϕ, and ψ; the reproducing kernel might not be able to reconstruct the high frequency/wave number part of the solution (second term in Eq. (5.5)); and these high frequency/wave number components can be readily picked up by multi-resolution wavelets analysis.

Presently, we are working on the theoretical analysis of this type of reproducing kernel methods. Upon the understanding of Eqs. (5.6), we shall implement the correct ϕ, and ψ into the continuous multiple-scale frequency bands approximation of the response:

$$u^h(x) = \int_V C(x, y, a_0, a^m)\, a_0^{-1}\, \phi\left(\frac{y-x}{a_0}\right) u(y)\, dy \qquad \text{low frequency band}$$

$$+ \sum_{m=1}^{M} \int_V C(x, y, a_0, a^m)\, a_0^{-m}\, \psi\left(\frac{y-x}{a^m}\right) u(y)\, dy \qquad \text{high frequency band} \tag{5.7}$$

Unlike orthogonal wavelets, equation (5.7) holds for arbitrary domains. Discretization of Eq. (5.7) gives the desired multi-grid/multi-resolution analysis of the complex dynamic systems:

$$u^h(x) = \sum_{J=1}^{NP0} [C(x, x_J, a_0, a^m)\, \Delta x_J\, u_J]\, a_0^{-1}\, \phi\left(\frac{x_J-x}{a_0}\right) \qquad \text{low frequency band}$$

scaling factor coefficients

$$+ \sum_{J=1}^{NP1} [C(x, x_J, a_0, a^m)\, \Delta x_J\, u_J]\, a^{-1}\, \psi\left(\frac{x_J-x}{a}\right) \qquad \text{1st higher frequency band}$$

1st-scale wavelet coefficients

$$\vdots$$
$$+$$

$$+ \sum_{J=1}^{NPM} [C(x, x_J, a_0, a^m)\, \Delta x_J\, u_J]\, a^{-M}\, \psi\left(\frac{x_J-x}{a^M}\right) \qquad M^{th} \text{ higher frequency band} \tag{5.8}$$

M^{th}-scale wavelet coefficients

It is noted that NPM ≥ ....≥ Np1 ≥ np0; and it constitutes an unstructured multi-grid analysis. We also wish to emphasize that orthogonal wavelets are not necessary; hence there is a larger class of window functions which can give good time and frequency localization.

6. Numerical Examples

The steady-state advection-diffusion problem can be stated for the one-dimensional case as follows:

$$u_{,xx} - a u_{,x} = b(x) \qquad \text{in } \Omega \tag{6.1}$$

with the boundary conditions

$$u(x_g) = u_1 \qquad \text{on } \Gamma_g \tag{6.2a}$$

$$u_{,x}(x_h) = u_2' \qquad \text{on } \Gamma_h \tag{6.2b}$$

where Ω is the domain (i.e., $0 \le x \le L$), Γ_g is the boundary within essential boundary conditions and Γ_h the boundary with natural boundary conditions. The whole boundary is $\Gamma = \Gamma_g \cup \Gamma_h$ and $\Gamma_g \cap \Gamma_h = \{\varnothing\}$. $(\ )_{,x}$ denotes derivatives with respect to x. u is the scalar unknown, a given constant, and b(x) a given source term. The parameter a is the advetive velocity divided by the diffusion coefficient. The Peclet number is therefore

$$Pe = \frac{a \Delta x}{2} \tag{6.2c}$$

The boundary conditions are given. This problem can be viewed as a heat transfer problem with convective and diffusive heat transfer. The source term b(x) can be caused by a chemical reaction. Following Hughes et. al. [9] the weak form of equation (6.1) with the least square term can be written as

$$\int_{\Omega} w\,(u_{,xx}-a\,u_{,x}-b)\,d\Omega + \int_{\Omega} (w_{,xx}-a\,w_{,x})\,\tau\,(u_{,xx}-a\,u_{,x}-b)\,d\Omega = 0 \qquad (6.3)$$

where w is an arbitrary test function and τ is a parameter. Using the approximations u^h and w^h for the functions u and w, we obtain the usual matrix equation.

The following numerical examples use a highly irregular source term to cause a nonlinear solution with two peaks. The source term consists of two terms that are very similar and summed together. Each part is

$$\begin{aligned} b_i(x) = {} & \frac{2c_1c_2e^{c_2(x-x_0)}\left(e^{2c_2(x-x_0)}-1\right)\mathrm{Sech}(c_1(x-x_0))^2}{\left(e^{2c_2(x-x_0)}+1\right)^2} \\ & + \frac{2c_1^2\,\mathrm{Sech}(c_1(x-x_0))^2\,\mathrm{Tanh}(c_1(x-x_0))}{\left(e^{c_2(x-x_0)}+e^{-c_2(x-x_0)}\right)} \\ & - \frac{c_2^2\left(e^{c_2(x-x_0)}+e^{-c_2(x-x_0)}\right)*\left(1-\mathrm{Tanh}(c_1(x-x_0))\right)}{\left(e^{c_2(x-x_0)}+e^{-c_2(x-x_0)}\right)^2} \\ & + \frac{2c_2^2\left(e^{c_2(x-x_0)}-e^{-c_2(x-x_0)}\right)^2*\left(1-\mathrm{Tanh}(c_1(x-x_0))\right)}{\left(e^{c_2(x-x_0)}+e^{-c_2(x-x_0)}\right)^3} \\ & + a\left(\frac{c_2\left(e^{c_2(x-x_0)}-e^{-c_2(x-x_0)}\right)\left(1-\mathrm{Tanh}(c_1(x-x_0))\right)}{\left(e^{c_2(x-x_0)}+e^{-c_2(x-x_0)}\right)^2} + \frac{c_1\,\mathrm{Sech}(c_1(x-x_0))^2}{\left(e^{c_2(x-x_0)}+e^{-c_2(x-x_0)}\right)}\right) \end{aligned} \qquad (6.4)$$

where the parameter x_0 governs the position of the peak, c_1 controls the sharpness on the right side of the peak and c_2 controls the decay on the left side. In the previous equation the second indice for the paramters x_0, c_1 and c_2 is omitted. Therefore $x_0 = x_{0i}$, $c_1 = c_{1i}$ and $c_2 = c_{2i}$ for i=1,2.

The resulting source term is

$$b(x) = k_1b_1(x) + k_2b_2(x) \qquad (6.5)$$

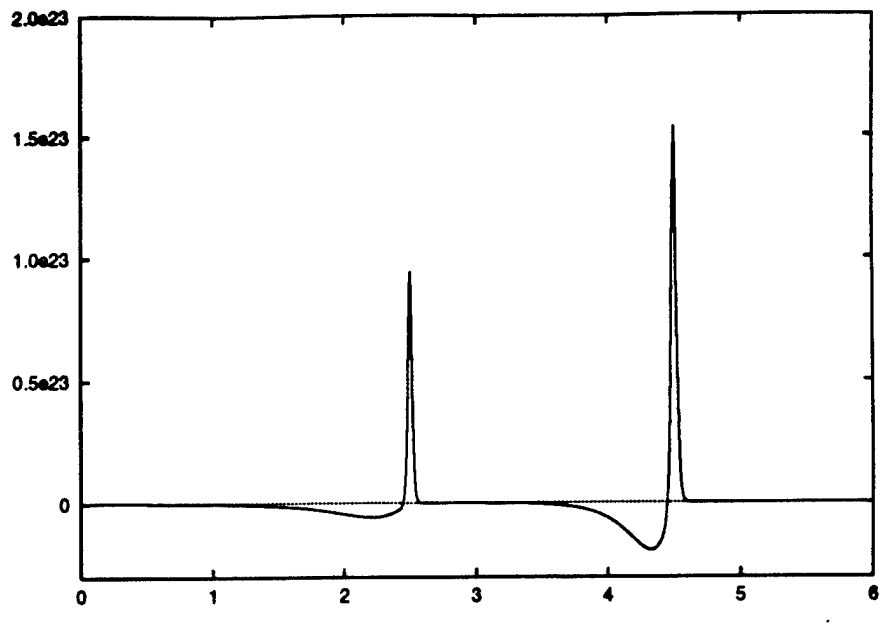

Figure 6.1 Source term used in the examples

with the parameters

i	1	2
x_{0i}	5.0	2.5
c_{1i}	50	50
c_{2i}	1.0	3.0
k_i	0.5	1.0

where the parameter k determines the size of the peak. The source term using these coefficients is shown in figure 6.1.

The homogeneous solution for the advection-diffusion equation on the domain $0 \le x \le 6$ with boundary conditions $u(0)=0$, $u(6) = 1$ becomes

$$u^H(x) = \frac{e^{ax} - 1}{e^{6a} - 1} \tag{6.6}$$

where the particular solution with b(x) given in (6.17)

$$u^P(x) = k_1 u_1^P(x) + k_2 u_2^P(x) \tag{6.7}$$

where

$$u_i^P(x) = \frac{1-\mathrm{Tanh}(c_1(x-x_0))}{e^{c_2(x-x_0)}+e^{-c_2(x-x_0)}} \qquad \text{for } i = 1,2 \tag{6.8}$$

with the appropriate constants from the table above. The parameter a is set to a=1000 in the following examples.

The results for the diffusion equation were obtained by setting the parameter a to zero and setting the boundary conditions to u(0)=0, u(6) = 0.

The results for the Reproducing Kernel Mothod are obtained by using a Window function W of the form

$$W(z) = e^{-z^2} \tag{6.9}$$

and

$$a_o = 2^j \Delta x \sqrt{\frac{2}{\pi}} \tag{6.10}$$

To show the influence of the parameter j, the solution of the differential equation is calculated for several j. Note that for j=-2.2 the solution becomes unstable and that for a j<0 the solution approaches the finite element solution.

Note that the wavelets are scaled with a factor Δx to scale the mother wavelet to the size of the mesh.

The solutions of the Diffusion Equation and the Advection Diffusion Equation using several different methods are shown in Figures 6.1 - 6.6 An error plot for the Diffusion Equation is shown in Figure 6.5. The solution for 31 nodes is not representative, the source term is underintegrated.

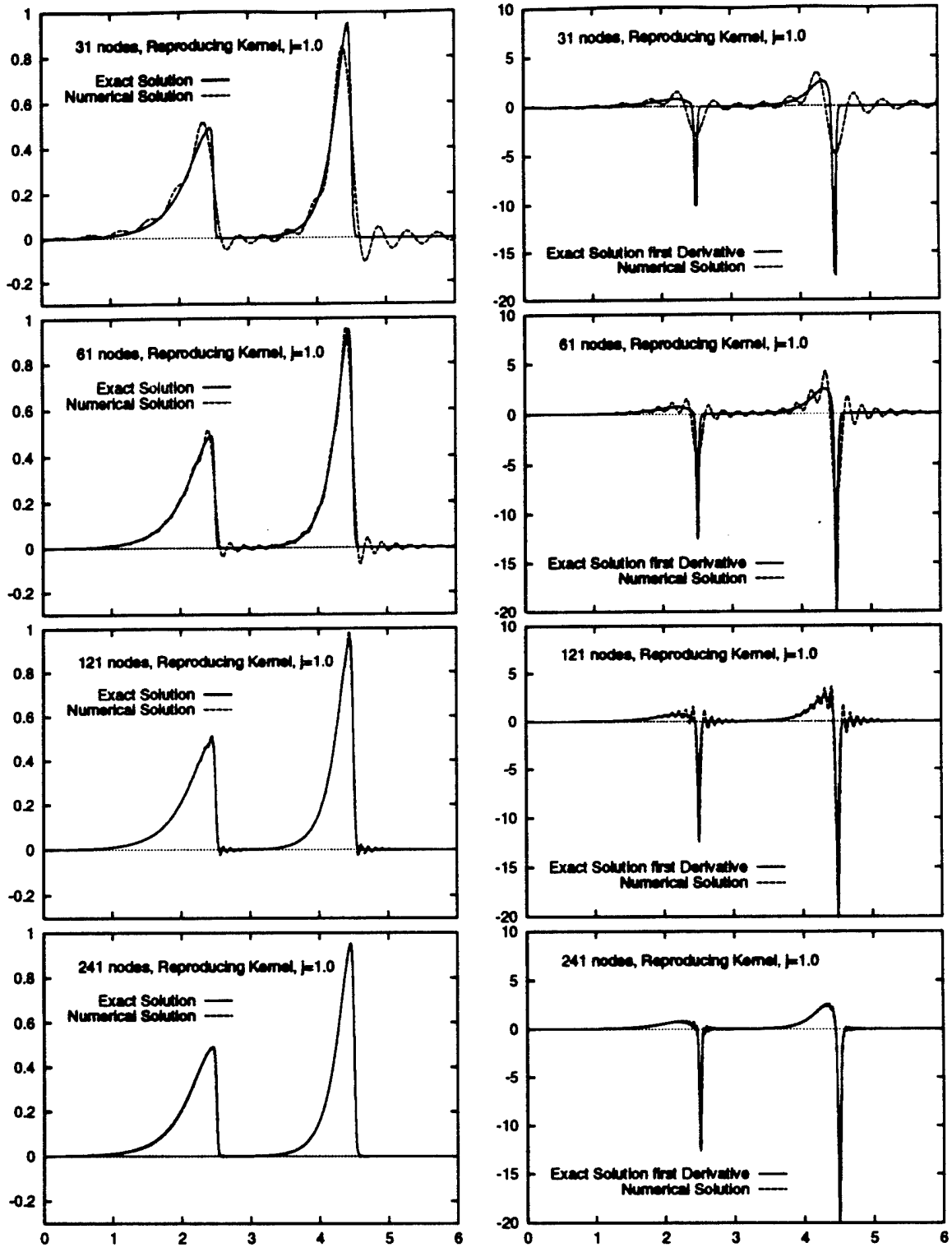

Figure 6.1 Solution of the Diffusion Equation
using Gaussian Reproducing Kernel with j= 1.0

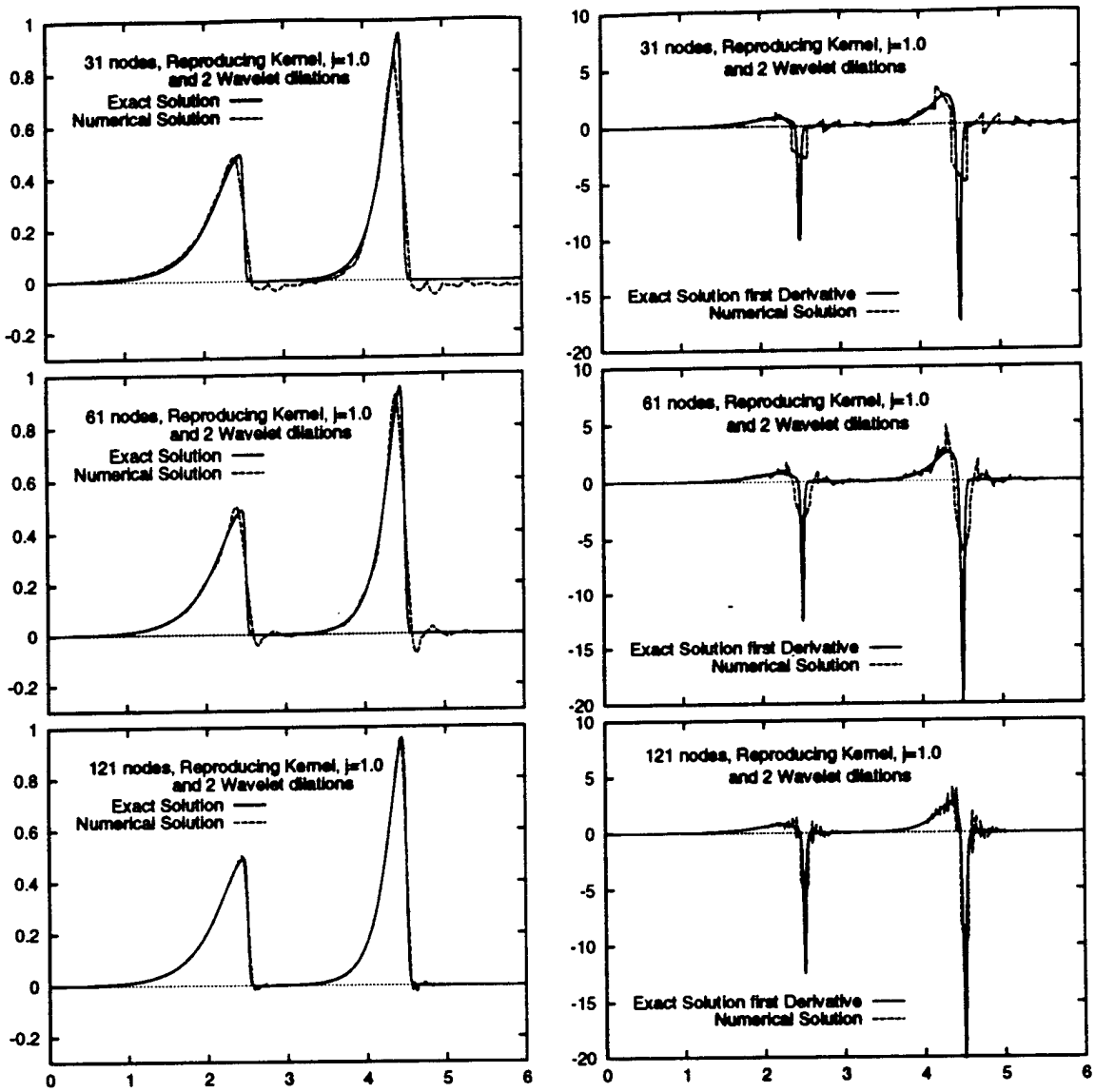

Figure 6.2 Solution of the Diffusion Equation
using two Wavelet dilations

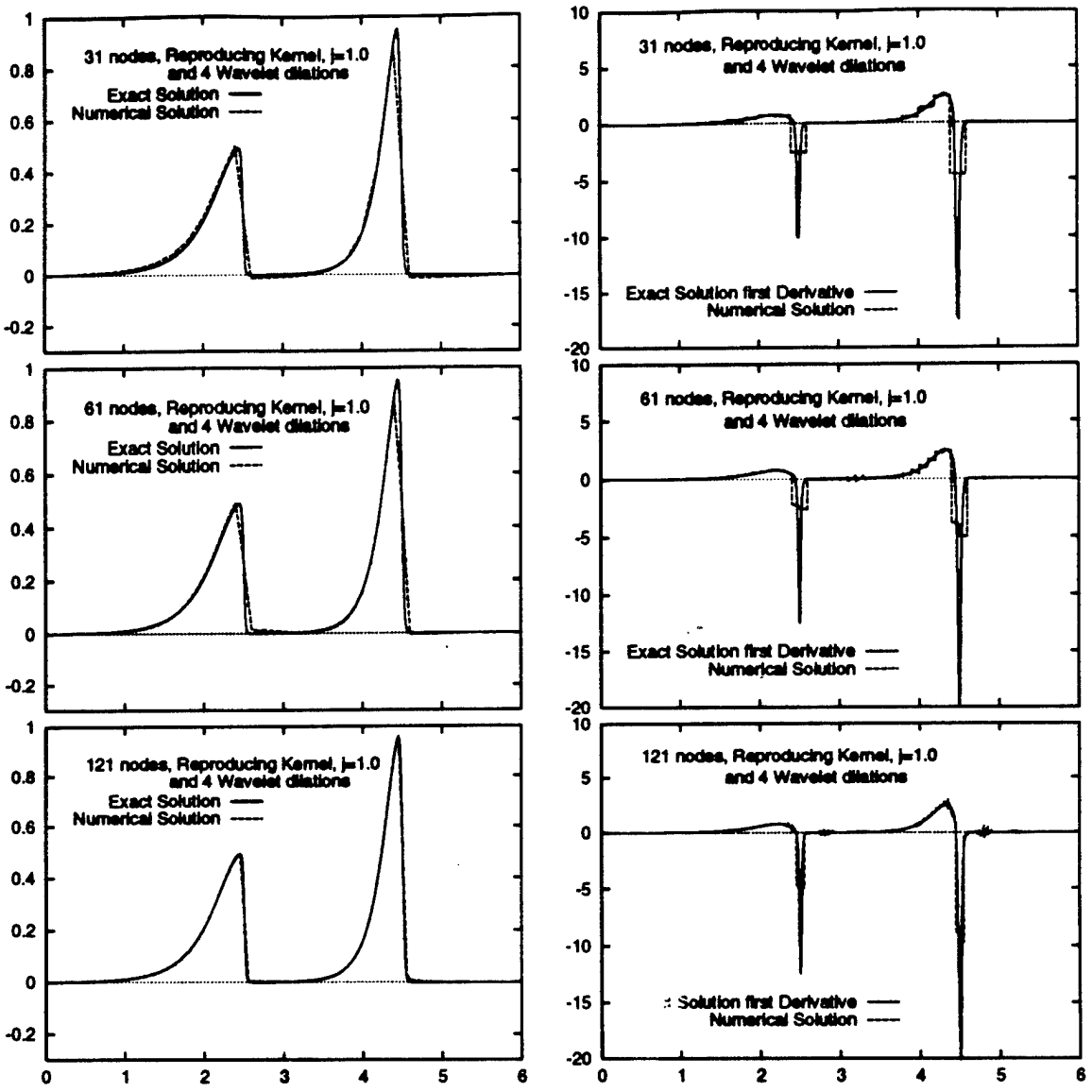

Figure 6.3 Solution of the Diffusion Equation
using four Wavelet dilations

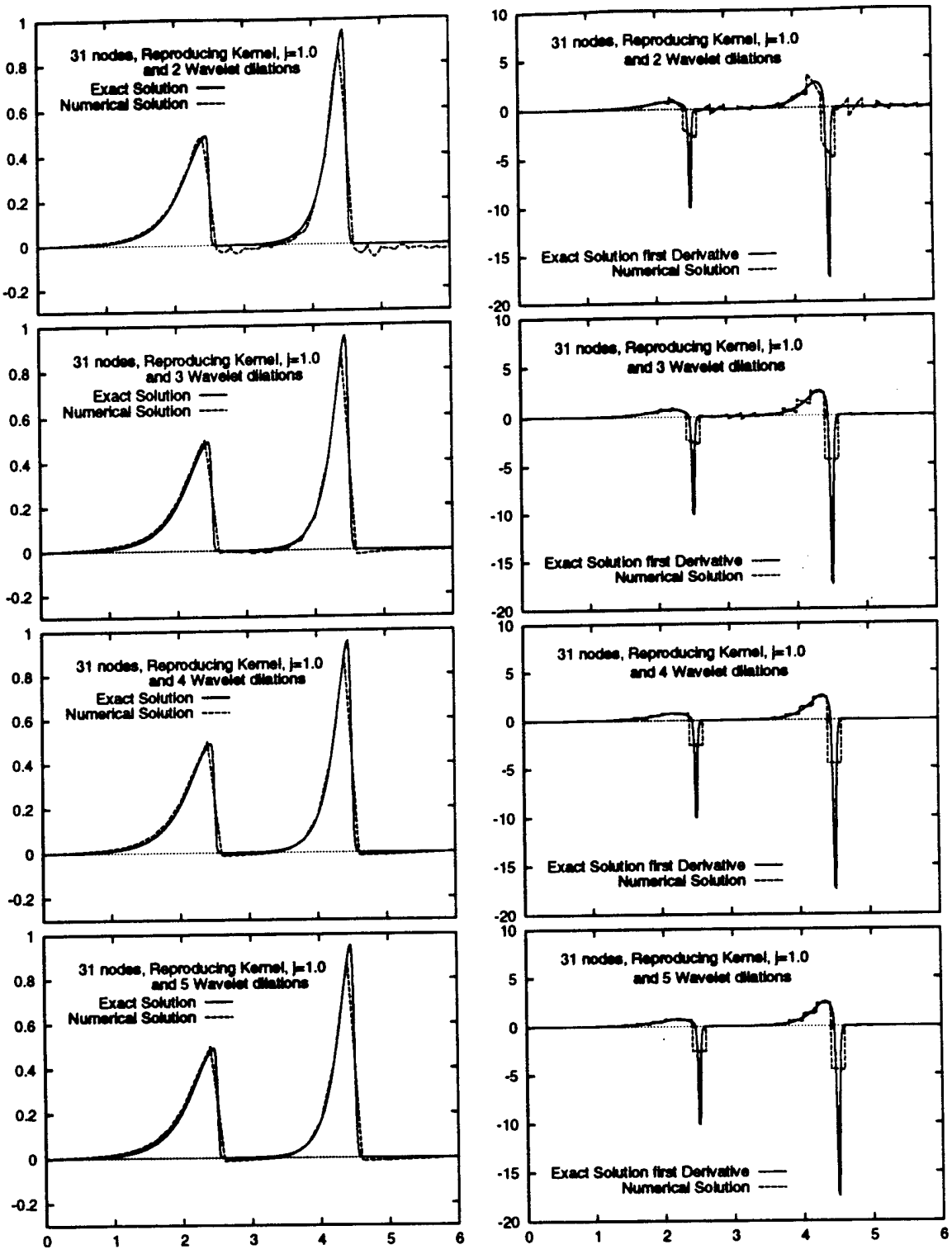

Figure 6.4 Solution of the Diffusion Equation
using 31 nodes and several number of Wavelet dilations

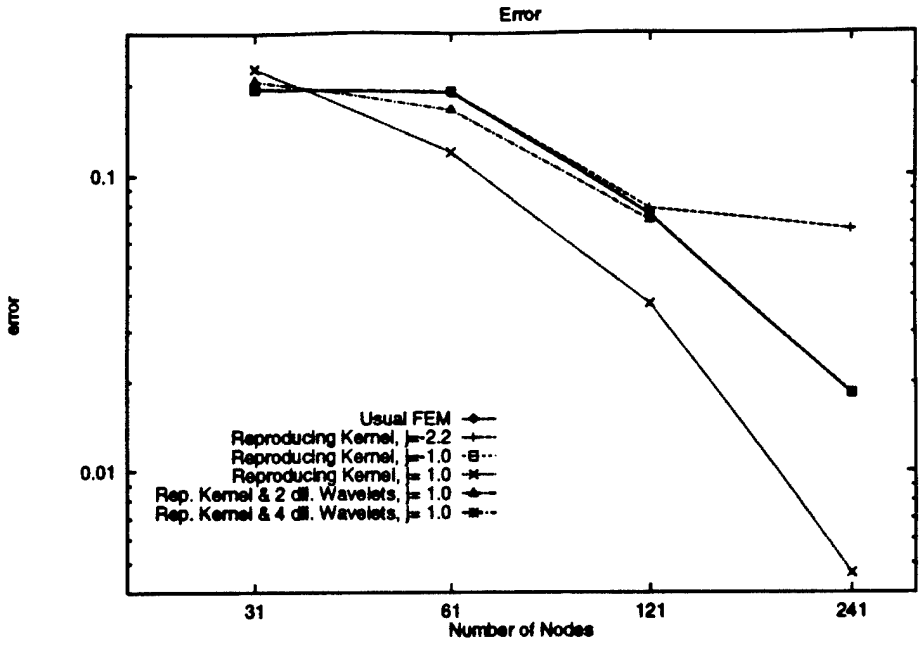

Figure 6.5a Error of numerical solutions for the Diffusion Equation

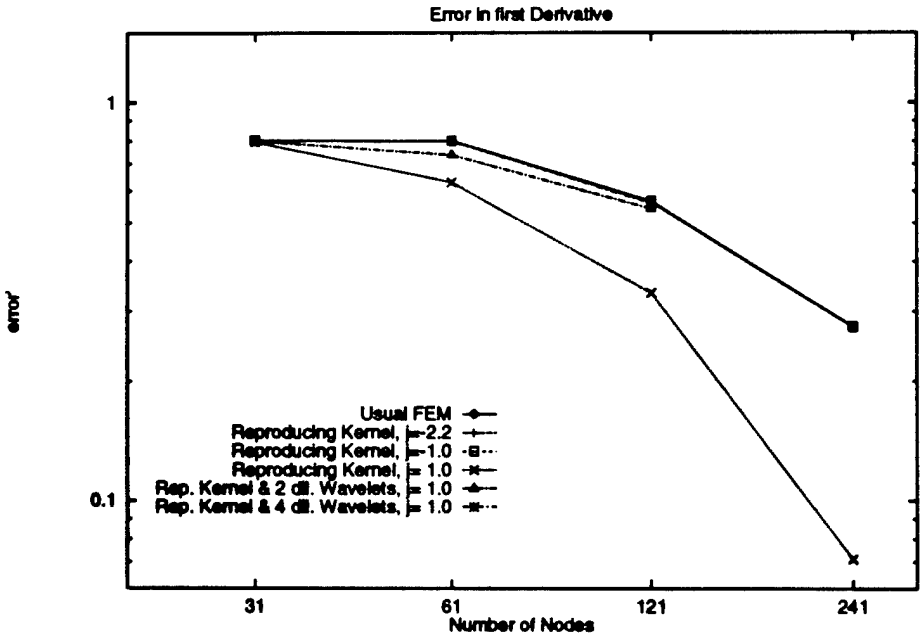

Figure 6.5b Error in the derivative of numerical solutions for the Diffusion Equation

num. of nodes	31	61	121	241
Usual FEM	0.19545	0.18977	0.07468	0.01827
RKPM j = -2.2	0.19511	0.18954	0.07829	0.06641
RKPM j = -1.0	0.19589	0.19054	0.07507	0.01839
RKPM j = 1.0	0.22884	0.11999	0.03746	0.00463
2 WL dil., j=1.0	0.20792	0.16593	0.07138	
4 WL dil., j=1.0	0.19507	0.19137	0.07507	

Table 6.1a Error of numerical solutions for the Diffusion Equation

num. of nodes	31	61	121	241
Usual FEM	0.80144	0.79926	0.56435	0.27424
RKPM j = -2.2	0.80144	0.79910	0.56383	0.27401
RKPM j = -1.0	0.80283	0.80029	0.56555	0.27422
RKPM j = 1.0	0.79341	0.63022	0.33317	0.07116
2 WL dil., j=1.0	0.79900	0.73682	0.54145	
4 WL dil., j=1.0	0.80149	0.79854	0.55935	

Table 6.1b Error in the derivative of numerical solutions for the Diffusion Equation

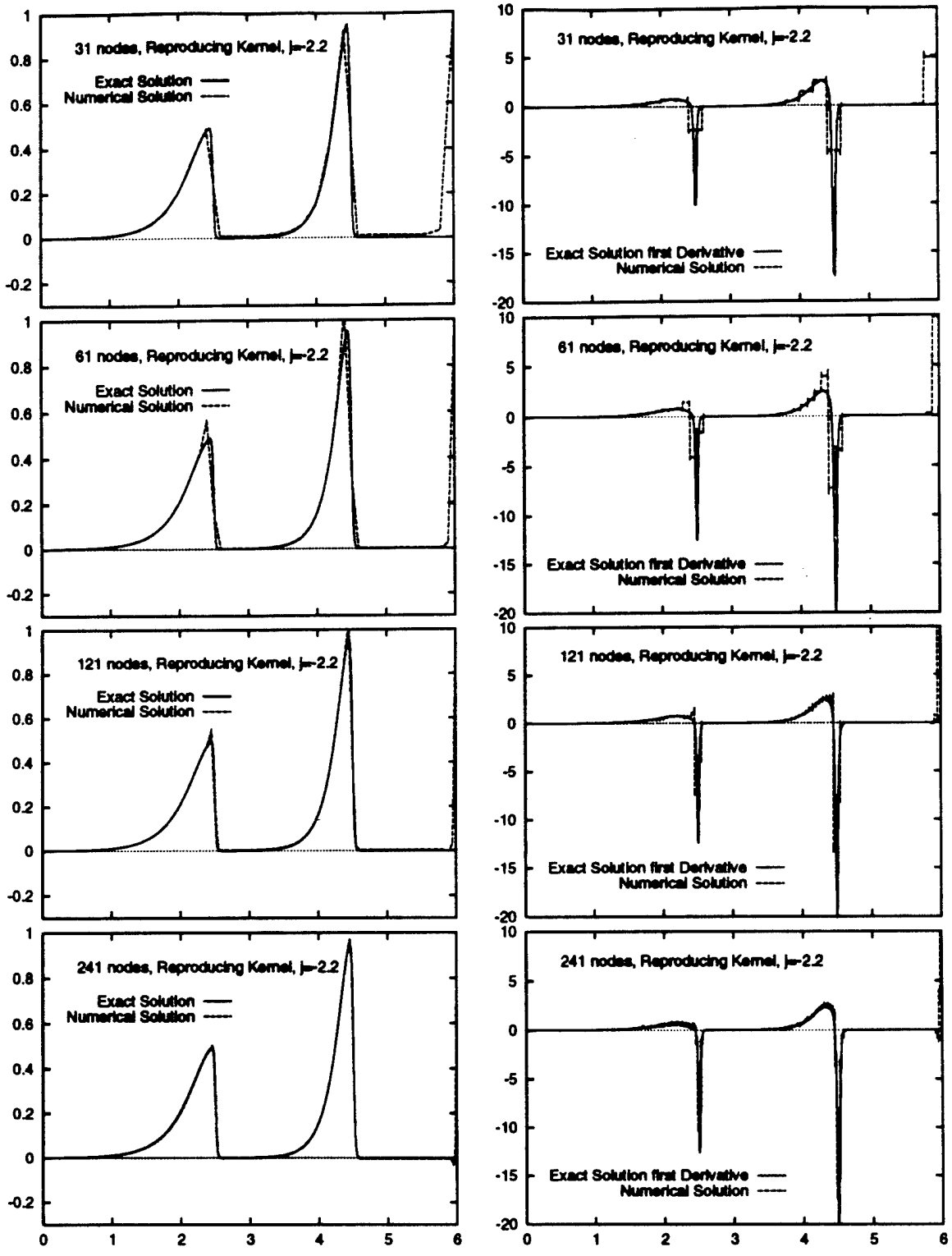

Figure 6.6 Solution of the Advection-Diffusion Equation using Gaussian Reproducing Kernel with j= -2.2

References

Amsden, A. A., and Harlow, F. H., [1970]; "The SMAC Method, A Numerical Technique for Calculating Incompressible Fluid Flow," Tech Report LA-4370, Los Alamos Scientific Laboratory.

Belytschko, T., "An Overview of Semidiscretization and Time Integration Procedures," Computer Methods for Transient Analysis, T. Belytschko and T. J. R. Hughes eds., North-Holland, Amsterdam, 1983, pp. 1-63.

Belytschko, T. and Kennedy, J. M., [1978]; "Computer Models for Subassembly Simulation," *Nuclear Engineering and Design*, **49**, pp. 17-38.

Belytschko, T., Lu, Y. Y. and Gu, L., [1993]; Element Free Galerkin Methods, (*preprint*).

Burton, D. E., and Harrison, A. K., [1991]; "Simulation of Single Mode Richtmyer-Meshkov Instability Using the Adaptive Free Lagrange Method," UCRL-JC-108033, LLNL report.

Chui, C. K., [1992]; *An Introduction to Wavelets*, Academic Press.

Daubechies [1992]; Ten Lectures on Wavelets, CBMS/NSF Series in Applied Mathematics, No. 61, *SIAM Publication.*

Gingold, R. A. and Monaghan, J. J., [1977]; Smoothed Particle Hydrodynamics: Theory and Application to Non-Spherical Stars, *Mon. Not. Roy. Astron. Soc.*, **181**, 375-389.

Gingold, R. A., and Monaghan, J. J., [1982]; "Kernel Estimates as a Basis for General Particle Methods in Hydrodynamics," *J. Comp. Physics*, **46**, pp. 429-453.

Gottlieb, D., and Orszag, S. A., [1977]; Numerical Analysis of Spectral Methods: Theory and Applications, *SIAM*, New York.

Harlow, F. H., Amsden, A. A., and Nix, J. R., [1976]; "Relativistic Fluid Dynamics Calculation with Particle-in-Cell Technique," *J. Comput. Phys.*, **20**.

Harlow, F. H., and Welch, J. E., [1965]; "Numerical Calculation of Time-Dependent Viscous Incompressible Flow of Fluid with Free Surface," *The Physics of Fluids*, **8**, 2182-2189.

Hirt, C. W., et al, [1975]; "SOLA - A Numerical Solution Algorithm for Transient Fluid Flows," Los Alamos Scientific Laboratory report LA-5852.

Hirt, C. W., [1983]; "Flow Analysis for Non-Experts," Engineering Foundation Conference Proceedings, Modeling and Control of Casting and Welding Processes II.

Huerta, A., and Liu, W. K., [1988]; "Viscous Flow with Large Free Surface Motion," *Computer Methods in Applied Mechanics and Engineering*, **69**, 277-324.

Hughes, T. J. R., [1987]; The Finite Element Method, *Prentice-Hall.*

Hughes, T. J. R., and Hulbert, G. M., [1988]; "Space-Time Finite Element Methods for Elastodynamics: Formulations and Error Estimates," *Computer Methods in Applied Mechanics and Engineering*, **66**, 339-363.

Johnson, G. R., Peterson, E. H. and Stryrk, R. A., [1993]; Incorporation of An SPH Option into The EPIC Code for A Wide Range of High Velocity Impact Computations, (*preprint*).

Lancaster, P. and Salkauskas, K., [1981]; Surfaces Generated by Moving Least Squares Methods, *Mathematics of Computation*, **37**, 141-158.

Libersky, L. D. and Petschek, A. G., [1990]; Smooth Particle Hydrodynamics With Strength of Materials, *Advances in the Free-Lagrange Method, Lecture Notes in Physics*, 248-257.

Liu, W. K., Zhang, Y. and Ramirez, M. R., [1991]; Multiple Scale Finite Element Methods, *International Journal for Numerical Methods in Engineering*, 32, 969-990.

Liu, W. K., et al., [1988]; "ALE Petrov-Galerkin Finite Elements for Nonlinear Continua," *Computer Methods in Applied Mechanics and Engineering*, **68**, 259-310.

W.K. Liu, et al., [1991]; "Adaptive ALE Finite Elements with Particular Reference to External Work Rate on Frictional Interface," *Computer Methods in Applied Mechanics and Engineering*, **93** ,189-216.

Lucy, L., [1977]; A Numerical Approach to Testing The Fission Hypothesis, *A. J.*, **82**, 1013-1024.

Monaghan, J. J., [1982]; Why Particle Methods Work, *SIAM J. Sci. Stat. Comput.*, **3**, 422-433.

Monaghan, J. J., [1988]; An Introduction to SPH, *Comp. Phys. Comm.*, **48**, 89-96.

Monaghan, J. J., and Gingold, R. A., [1983]; "Shock Simulation by the Particle Method SPH," *J. Comp. Physics*, **52**, pp.374-389.

Nayroles, B., Touzot, G. and Villon, P., [1992]; Generalizing The Finite Element Method: Diffuse Approximation and Diffuse Elements, *Computational Mechanics*, **10**, 307-318.

Nichols, B. D., and Hirt, C. W., [1971]; "Improved Free Surface Boundary Conditions for Numerical Incompressible Flow Calculations," *J. Comp. Phy.*, **8**.

Shakib, F., and Hughes, T. J. R., [1991]; "A New Finite Element Formulation for Computational Fluid Dynamics: IX. Fourier Analysis of Space-Time Galerkin/Least-Squares Algorithms," *Computer Methods in Applied Mechanics and Engineering*, **87** ,35-58.

Subbiah, S., et al, "Non-isothermal flow of polymers into two-dimensional, thin cavity molds: a numerical grid generation approach," *Int J. Heat Mass Transfer*, **32/3**, 415-434, 1989.

Tezduyar, T. E., Behr, M., and Liou, J., [1992]; "A New Strategy for Finite Element Computations Involving Moving Boundaries and Interfaces - the Deforming-Spatial-Domain/Space Tine Procedure: I. The Concept and the Preliminary Tests," *Computer Methods in Applied Mechanics and Engineering*, **94** ,339-351.

The Following papers have been presented at the 1993 ASME Winter Annual Meeting in New Olreans. These papers (2) are being extended and will be submitted for possible publication in International Journals.

(1) Liu, W. K., Adee, J., Jun, S., and Belytschko, T., "Reproducing Kernel Particle Methods for Elastic and Plastic Problems," , *Advanced Computational Methods for Material Modeling*, Eds. Benson, D. J. , and Asaro, R. A., AMD 180 and PVP 268, ASME, pp. 175-190, 1993.

(2) Liu, W. K., and Oberste-Brandenburg, C.,"Reproducing Kernel and Wavelet Particle Methods," *Aerospace Structures: Nonlinear Dynamics ans System Response*, Eds. Cusumano, J. P., Pierre, C., and Wu, S. T., AD 33, ASME, pp. 39-56, 1993.

The following papers have been or will be submitted to **Journals** for possible publications.

(1) Liu, W. K., Zhang, Y. F., Belytschko, T., Jun, S., Adee, J., and Gu, L., "Reproducing Kernel Particle Methods," submitted to *International Journal of Numerical Methods in Fliuds*.

(2) Liu, W. K., Chen, Y. J., and Oberste-Brandenburg, C.,"Reproducing Kernel and Wavelet Particle Methods," under preparation.

(3) Liu, W. K., Adee, J., Jun, S., and Belytschko, T., "Reproducing Kernel Particle Methods for Structural Dynamics," under preparation.

The above three papers are given below.